Identification of alprenolol hydrochloride as an anti-prion compound using surface plasmon resonance imaging

Yukiko Miyazaki[1,2], Takeshi Ishikawa[2,3], Yuji O. Kamatari[4], Takehiro Nakagaki[1], Hanae Takatsuki[5], Daisuke Ishibashi[1], Kazuo Kuwata[6], Noriyuki Nishida[1#*], Ryuichiro Atarashi[5#*]

[1]Division of Molecular Microbiology, [3]Molecular Epidemiology, Graduate School of Biomedical Sciences, Nagasaki University, Japan.

[2]Program for Nurturing Global Leaders in Tropical and Emerging Infectious Diseases, Graduate School of Biomedical Sciences, Nagasaki University, Japan.

[4]Life Science Research Center, Gifu University, Japan

[5]Division of Microbiology, Department of Infectious Diseases, Faculty of Medicine, University of Miyazaki, Japan.

[6]United Graduate School of Drug Discovery and Medical Information Sciences, Gifu University, Japan

[#]These authors contributed equally to the study.

*Corresponding authors

E-mail: noriyukinishida@icloud.com Tel.: +81-95-819-7059 Fax: +81-95-819-7060

E-mail: ryuichiro_atarashi@med.miyazaki-u.ac.jp Tel.: +81-985-85-0871 Fax: +81-985-85-6475

Acknowledgments

We thank Atsuko Matsuo for technical assistance. This work was supported by JSPS KAKENHI Grant Number JP15H04269 and a grant form Takeda Science Foundation.

We thank Kate Fox, DPhil, from Edanz Group (www.edanzediting.com/ac) for editing a draft of this manuscript.

Abstract

Prion diseases are transmissible neurodegenerative disorders of humans and animals, which are characterized by the aggregation of abnormal prion protein (PrP^{Sc}) in the central nervous system. Although several small compounds that bind to normal PrP (PrP^{C}) have been shown to inhibit structural conversion of the protein, an effective therapy for human prion disease remains to be established. In this study, we screened 1200 existing drugs approved by the US Food and Drug Administration (FDA) for anti-prion activity using surface plasmon resonance imaging (SPRi). Of these drugs, 31 showed strong binding activity to recombinant human PrP, and three of these reduced the accumulation of PrP^{Sc} in prion-infected cells. One of the active compounds, alprenolol hydrochloride, which is used clinically as a β-adrenergic blocker for hypertension, also reduced the accumulation of PrP^{Sc} in the brains of prion-infected mice at the middle stage of the disease when the drug was administered orally with their daily water from the day after infection. Docking simulation analysis suggested that alprenolol hydrochloride fitted into the hotspot within mouse PrP^{C}, which is known as the most fragile structure within the protein. These findings provide evidence that SPRi is useful in identifying effective drug candidates for neurodegenerative diseases caused by abnormal protein aggregation, such as prion diseases.

Keywords

Prion diseases; Surface plasmon resonance imaging; Alprenolol hydrochloride; Docking simulation

Introduction

Prion diseases are transmissible neurodegenerative disorders, which include Creutzfeldt-Jakob disease (CJD) and Gerstman-Sträussler-Scheinker disease in humans, scrapie in sheep and bovine spongiform encephalopathy (BSE) in cattle. The infectious agent responsible for these diseases is misfolded and aggregated prion protein (PrP^{Sc}), which is generated by conformational changes in cellular prion protein (PrP^{C}) [1,2].

Effective therapeutics have not been established for human prion diseases, despite decades of research. The drugs that have been identified target several different stages of the prion infection process: conformation changes in PrP, clearance of aggregated PrPs and signaling pathways leading to neurodegeneration [3-5]. Quinacrine inhibited the conversion process by binding to PrP^{C}, leading to reduced PrP^{Sc} accumulation in prion-infected cultured cells [6,7]; however, it exhibited nonsignificant therapeutic effects on CJD patients and showed side effects such as liver dysfunction and skin rashes [8,9]. Pentosan polysulfate was also reported to suppress PrP conversion by interfering with the interaction between PrP^{C} and PrP^{Sc} [10,11]. Intraventricular infusion of pentosan polysulfate significantly prolonged survival in animals [12,13], but also showed adverse effects such as seizures due to the slow metabolism of the drug [13], and therefore this drug was not approved for human use, even by intraventricular

71 administration [14,12]. Doxycycline was effective in prion-infected cultured cells and in
72 animals, but its administration did not affect the survival time of CJD patients [15-17].
73 Anti-PrP antibodies prevented prion pathogenesis in mice, but problems such as
74 neurotoxicity and impermeability to the blood–brain barrier were encountered [18-21].
75 Several compounds targeting intracellular protein degradation systems, such as
76 autophagy or signaling pathways related to the unfolded protein response, were reported
77 to show anti-prion effects [22-24]. However, some of these led to toxicity in humans
78 because they also acted on the original molecular functions in normal tissues and cells,
79 leading to the disruption of cellular homeostasis [24,25].

80 Recently, *in silico* studies have been conducted to identify novel PrP-binding
81 compounds. Hotspot residues responsible for conformational changes in PrP^{C} were
82 identified, and a lead compound designated GN8 was characterized as an anti-prion
83 compound that interacts with this site [26]. Based on these findings, further studies
84 involving a structure-based drug discovery approach using docking simulations
85 identified drug candidates that targeted the hotspot and exerted anti-prion effects on
86 prion-infected cells and mice [27,28]. In this study, we conducted screening of 1,200
87 FDA-approved drugs by surface plasmon resonance imaging (SPRi) to identify
88 molecules able to bind to recombinant PrP. SPRi has recently been developed to

89 overcome the limitation of conventional SPR in terms of high-throughput screening.
90 Conventional SPR involves only a small number of flow cells on its sensor chip,
91 whereas SPRi can visualize the whole surface image of a sensor chip to detect reflection
92 changes arising from molecular binding events between immobilized small molecules
93 and flowing proteins via the use of a charge-coupled device (CCD) camera. SPRi
94 therefore allows for multiplex detection and high throughput screening of molecular
95 interactions by a single run using an array format sensor chip [29,30]. This reverse SPR
96 technology has been used to identify binding molecules to specifically target proteins
97 [31,29]. After SPRi screening, we evaluated the anti-prion activity of the hit compounds
98 by quantifying PrP^{Sc} in prion-infected cultured cells and mice.
99
100 **Results**
101 **Screening of the drug by SPR imaging**
102 The 1200 FDA-approved drugs were screened to identify compounds with binding
103 activity to human PrP^{C} using the Plexera PlexArray system. Recombinant human PrP
104 90–231 ($rHuPrP_{90–231}$) was applied to the library compounds immobilized on a sensor
105 chip, and each affinity was measured. Thirty-one compounds showed dissociation
106 constant (K_D) values of less than 1×10^{-6} M (Table 1), with dequalinium dichloride,

alexidine dihydrochloride and esmolol hydrochloride having the highest order K_D values (10^{-10}). Amphotericin B, which has been reported to inhibit PrP^{Sc} generation in scrapie-infected cultured cells and to prolong the course of the disease in animals [32,33], was also shown to exhibit binding activity to PrP^{C}.

Anti-prion effects of the hit compounds on prion-infected cultured cells

The inhibitory effects of the 31 hit compounds on prion-infected culture cells were examined using N2a58 cells persistently infected with Fukuoka-1 strain (Supplementary Fig. 1). The cells were incubated with each compound for 48 hours at the indicated concentration, then the amount of PrP^{Sc} was quantified by western blotting after proteinase K digestion. We found that three compounds, alprenolol hydrochloride (Alp), bisoprolol fumarate (Bis) and colistin sulfate significantly reduced the level of PrP^{Sc} in the cultured cells (Fig. 1b). In addition, PrP^{Sc} completely disappeared after continued passage in the presence of Alp and Bis (Fig. 1d), both of which are β-adrenergic blockers used for the treatment of cardiovascular diseases. In particular, Alp exhibited strong anti-prion effects, with an IC_{50} value of 15 μM (Fig. 1c). Esmolol hydrochloride and oxprenolol hydrochloride (Oxp), that are also β-adrenergic blockers with similar structures to Bis and Alp respectively (Fig. 1a), did not exert anti-prion effects on the infected cells (Fig. 1e). The effect of colistin on prions was evident but weaker than that

125 of Alp or Bis. The inhibitory effect of antimycin A, a mitochondrial inhibitor, could not
126 be evaluated due to its potent cytotoxicity on prion-infected cultured cells.

127 **Alprenolol hydrochloride reduces PrP^{Sc} in the brains of prion-infected mice**

128 To evaluate the *in vivo* therapeutic effects of the identified anti-prion compound,
129 animal experiments using prion-infected mice were performed. As Alp can penetrate the
130 blood–brain barrier easier than Bis [34,35], Alp was selected for the animal experiments.
131 CD-1 mice intracerebrally infected with mouse-adapted human prion, Fukuoka-1, were
132 orally administered drinking water containing Alp at 50 mg/L or 250 mg/L from the day
133 after infection (half-life of Alp: ~2 hours) [35]. At 115 days post infection (d.p.i.), some
134 of the mice (Control: n = 3; 250 mg/L: n = 5; 50 mg/L: n = 3) showing no symptoms of
135 prion disease were euthanized to evaluate PrP^{Sc} accumulation and spongiform changes
136 in the brain tissue. PrP^{Sc} levels in the mice treated with Alp were significantly lower
137 than those of the control group (Fig. 2a). Immunohistochemistry showed reduced levels
138 of PrP^{Sc} staining in brain sections from Alp-treated mice as compared with the control
139 (Fig. 2b). There was a statistically significant decrease in the number of vacuoles in the
140 cortex from the mice treated with 50 mg/L of Alp (Fig. 3a). Although there appears to
141 be a dose-dependent decrease in the thalamus, the differences did not reach statistical
142 significance. These results suggest that Alp has an inhibitory effect on PrP^{Sc}

accumulation and spongiform changes in the mouse brain tissues at the middle stage of the disease (115 d.p.i). Whereas, the survival periods of the treated groups remained unchanged compared with the control (Fig. S2a, Table 2). In addition, similar levels of PrP^{Sc} accumulation and spongiform changes were observed in both groups at the terminal stage (Fig. S2b, c).

Conventional SPR and NMR analysis using alprenolol hydrochloride and recombinant PrP

We investigated the binding kinetics of Alp and Bis to recombinant mouse PrP 23–231 ($rMoPrP_{23–231}$) by conventional SPR analysis using the Biacore T200 system (Fig. S3). In contrast to the previous screening by SPRi, the proteins were immobilized on a sensor chip as ligands and the compounds were injected into this system. The K_D value of the positive control, quinacrine, was 0.69 mM (Fig. S3b), whereas ampicillin, which is not known to have any anti-prion effects, had a low binding affinity to $rMoPrP_{23-231}$ (Fig. S3a). The K_D values of Alp and Bis could not be calculated due to their low binding ability (Fig. S3b). Analysis using $rHuPrP_{23-231}$ as the ligand also presented similar results (Fig. S4). In NMR analysis, there was no difference in the spectra of $rMoPrP_{121-231}$ with or without Alp, suggesting that the interaction between Alp and $rMoPrP_{121-231}$ was not detectable at pH 4.8 (Fig. S5).

Docking simulation of the binding structures of alprenolol and PrP^C

To examine the binding structures of Alp with mouse PrP^C, we performed docking simulation using the software, AutoDock 4.2 [36]. In Figure 4, the binding structures obtained from the docking simulation are presented for Alp and Oxp and their enantiomers. The calculated binding positions were located around the helix-B for all of the molecules. This position was similar to the binding sites of other compounds that have previously been reported to have anti-prion activity [26,28]. We noted that Alp (Fig. 4a) displays an additional interaction with a loop near helix-A, resulting in the formation of a bridging conformation. By contrast, Oxp, which had no anti-prion effect on the infected culture cells regardless of its structural similarities to Alp (Fig. 1a, e), did not show a clear interaction with regions other than helix-B. The calculated binding energies of Alp (-5.68 and -5.81 kcal/mol) were lower than those of Oxp (-5.22 and -4.83 kcal/mol) indicating the higher affinity of Alp.

Discussion

In this study, we found that among the 31 compounds from the FDA-approved drug library showing binding activity in SPRi, three drugs, namely Alp, Bis and colistin sulfate, exhibited anti-prion effects on prion-infected cultured cells. This type of drug

179 repositioning approach can be promising because the safety and pharmacokinetics of
180 existing drugs have already been fully determined. This approach avoids the risks of
181 unknown adverse effects and saves considerable time and expense compared with *de*
182 *novo* drug development [37]. Indeed, drug repositioning has been proposed for the
183 development of drugs to treat prion diseases [22,38].

184 In the first screening, we used the SPRi system to identify PrP-binding compounds
185 from the drug library. Although Alp showed strong binding to $rHuPrP_{90–231}$ in this
186 screening, much lower binding ability to both $rMoPrP_{23–231}$ and $rHuPrP_{23–231}$ was
187 detected by conventional SPR analysis using the Biacore T200. As mentioned above,
188 both of the SPR systems detected binding affinity between proteins and compounds
189 based on reverse SPR mechanisms [30], which might explain the inconsistent results.
190 The sensitivity of SPR was thought to depend on the mass of the analytes that bind to
191 the ligands on the sensor chip. Higher molecular weight molecules induce larger
192 reflection changes and are therefore more readily detected than small molecules. Since
193 soluble proteins were used as analytes in SPRi, this assay might have relatively high
194 sensitivity in the detection of molecular interactions compared with conventional SPR.
195 However, both of the SPR technologies do not completely reproduce true physiological
196 events *in vivo* because the proteins or compounds are chemically immobilized on a

197 sensor chip in these systems. Moreover, little differences in the spectra of rMoPrP$_{121–231}$
198 with or without Alp were detectable by NMR analysis. It should be noted that NMR
199 analysis was conducted only under acidic conditions (pH 4.8) due to the solubility of
200 rMoPrP, making it difficult to determine the interaction between PrP and Alp under
201 physiological pH conditions. Together, there is no clear evidence to prove that the
202 anti-prion activity of Alp on infected cells and mice was attributed to its binding to
203 PrP^{C}; however, the docking simulation suggests that Alp interacts with the hotspot of
204 mouse PrP^{C}. This position is reported to be unstable and critical for pathogenic
205 conversion of PrP [26,39]. Notably, Oxp, which is similar in structure to Alp but has
206 lower affinity, exhibited no inhibitory effects on PrP^{Sc} accumulation in prion-infected
207 cells. The difference in structures between Alp and Oxp is only the integration of an
208 oxygen into a side chain (Fig. 1a), suggesting that the structure of this side chain is
209 important for the anti-prion effects of Alp. Alp formed a bridging conformation between
210 helix-B and a loop near helix-A in the docking simulation. However, neither Oxp nor its
211 enantiomer showed a clear interaction with regions other than helix-B. It has been
212 reported that GN8 disrupts the salt bridge between Arg156 at the C-terminus of helix-A
213 and Glu196 in the loop between helix-B and helix-C and rearranges this interaction,
214 leading to the conformational stability of PrP^{C} [39]. Our results suggest that the bridge

structure formed by Alp might contribute to its anti-prion effects, similar to GN8. However, it is possible that Alp may have another target responsible for its anti-prion effects as well as PrP^C. Although esmolol hydrochloride and Oxp are also β-adrenergic blockers, neither presented clear inhibition of prion-infected cultured cells, indicating that β-adrenergic receptors are unlikely to be the targets of Alp. Further studies are required to reveal the underlying mechanisms of the anti-prion effects of Alp.

The reduction in PrP^{Sc} accumulation in the brains of Alp-treated mice at 115 d.p.i. was confirmed by western blotting and immunohistochemical staining. By contrast, Alp treatment did not prolong the survival periods. The inconsistencies in the data may be attributed in part to the remarkable reduction in water intake by the infected mice at the terminal stage. However, further studies are needed to assess the inhibitory effects of Alp on prion diseases under different experimental conditions such as other routes, doses, start points and frequencies of Alp administration.

In conclusion, we identified PrP-binding compounds by SPRi screening. Among them, Alp showed anti-prion effects on prion-infected cultured cells and partially effects in mice. This SPRi approach is thought to be suitable for discovering effective drugs to treat neurodegenerative diseases caused by abnormal protein aggregation, such as prion diseases.

Methods

Compounds

Esmolol hydrochloride, dequalinium dichloride, fosinopril, antimycin A, and oxprenolol hydrochloride were purchased from Santa Cruz Biotechnology. Alexidine dihydrochloride, merbromin, candesartan, amphotericin B, alprenolol hydrochloride, triprolidine hydrochloride, methacycline hydrochloride, cefixime, and ethacrynic acid were purchased from Sigma-Aldrich. Demecarium bromide and cefoperazone were purchased from AK Scientific. Bisoprolol fumarate was purchased from MedChem Express. Benzbromarone, etifenin, cefotetan, and rebamipide were purchased from Tokyo Chemical Industry Co., Ltd. Atractyloside potassium salt was purchased from Toronto Research Chemicals. Furosemide and indomethacin were purchased from Nacalai Tesque. Acemetacin, ketoprofen, bumetanide, colistin sulfate, tranilast, norfloxacin, and doxepin hydrochloride were purchased from LKT Laboratories, Inc.

Cell culture

Mouse neuroblastoma Neuro 2a (N2a) cells were obtained from the American Type Culture Collection (CCL 131). N2a-FK cells are PrP^{C}-overexpressing N2a cells (N2a58 cells) that are persistently infected with mouse-adapted Gerstmann–Sträussler–

Scheinker strain, Fukuoka-1, as previously described. They were cultured at 37 °C under 5% CO_2 with Dulbecco's modified Eagle's medium (Wako), including 10% heat-inactivated fetal bovine serum, 100 units/mL penicillin and 100 μg/mL streptomycin (Nacalai Tesque).

Cell-based screening of the compounds

N2a-FK cells were seeded on 12 well plates at 1.5×10^5 cells/well. The next day, the cells were washed with PBS and the medium was replaced with fresh medium containing each of the sample compounds. Medium containing DMSO for the DMSO-dissolved compounds or water for the water-dissolved compounds was added to the control wells. After 48 hours of incubation, the cells were washed with PBS and lysed with lysis buffer (50 mM Tris-HCl pH 7.5, 150 mM NaCl, 0.5% Triton X-100, 0.5% sodium deoxycholate, 2 mM EDTA). Then the lysate was centrifuged for 1 min at 5,000 rpm and the supernatant was collected for immunoblotting.

In addition, N2a-FK cells were cultured in medium mixed with 50 μM of alprenolol hydrochloride, 100 μM of bisoprolol fumarate or 100 μM of colistin sulfate, and passaged every 3 days. As a negative control, N2a-FK cells were cultured in original medium. The cell lysates were collected every passage and total protein was prepared as described above.

Animal infection experiments

Three-week-old CD-1 mice were purchased from SLC (Hamamatsu, Japan). They were intracerebrally inoculated with 20 μl of 10% (w/v) brain homogenate from the affected mice with Fukuoka-1 at four weeks of age. The day after infection, the powdery components of Skajilol capsules (Kotobuki Pharmaceutical Co., Ltd), which contain alprenolol hydrochloride as a major active constituent, were added to the drinking water at 250 mg/L or 50 mg/L. Mice in the control group were given drinking water without the drug. At 115 d.p.i or the terminal stage, some of mice in each group were dissected to separate out their brain tissues (at 115 d.p.i., control: n = 3; 250 mg/L: n = 5; 50 mg/L: n = 3, at the terminal stage, control: n = 4; 250 mg/L: n = 4; 50 mg/L: n = 4). All of these experiments were approved by the Committee on the Animal Care and Use Committees of Nagasaki University. The mice were cared for according to the Guidelines for Animal Experimentation of Nagasaki University.

Preparation of brain homogenates

Mouse brain tissues were homogenized in PBS at 20% (w/v) by Multi-Beads Shocker (Yasui Kikai). Then, 10% brain homogenates for immunoblotting were prepared by mixing with an equal volume of 2 × lysis buffer.

Immunoblotting

The total protein concentration contained in the cell lysates and the brain homogenates was measured using the BCA Protein Assay Kit (Pierce). To digest PrP^C, the samples were reacted with 20 μg/ml Proteinase K (PK) for 30 min at 37°C. After denaturation by SDS sample buffer (50 mM Tris-HCl pH 6.8, 5% glycerol, 1.6% SDS, 100 mM dithiothreitol) for 10 min at 95°C, 100 μg (cell lysates) or 50 μg (brain homogenates) of each sample was applied to 15% acrylamide gel for SDS-PAGE. The protein bands were then transferred to PVDF membrane. For blocking, the membrane was placed in 5% (*w/v*) skim milk with TBST (10 mM Tris-HCl pH 7.8, 100 mM NaCl, 0.1% Tween 20) for 1 hour. For PrP detection, the membrane was then incubated with primary antibodies: M-20 (Santa Cruz Biotechnology) or SAF83 (SPI-Bio) diluted with 1% skim milk. Then, the membrane was further reacted with secondary antibodies: horseradish peroxidase-conjugated anti-goat (Santa Cruz Biotechnology) or anti-mouse IgG antibodies (GE Healthcare Life Sciences) diluted with 1% skim milk, and the bands were visualized using the ECL Prime Western Blotting Detection Kit (GE Healthcare Life Sciences) or Clarity Wester ECL Substrate (BioRad). The intensity of each band was quantified using the ImageJ software (National Institutes of Health).

Histopathological analysis

The hemispheres of fixed mouse brain tissues in 10% neutral buffered formalin were

305 embedded in paraffin after dehydration treatment. The paraffin blocks were sliced into
306 3-μm slices and the slices were placed on microscope slides. After deparaffinization,
307 hematoxylin-eosin staining was performed to evaluate the level of spongiform change.
308 To quantify the area occupied by vacuolation, the white areas in an image (670 μm ×
309 890 μm) from each brain region (cortex, thalamus, hippocampus, and striatum) were
310 measured using the ImageJ software and compared with the whole area of the image.
311 The hydrolytic autoclaving and formic acid method for PrP^{Sc} immunohistochemical
312 staining has been described previously [40].

313 **Preparation of recombinant PrP**

314 Expression and purification of recombinant human PrP 90–231 ($rHuPrP_{90–231}$),
315 recombinant human PrP 23–231 ($rHuPrP_{23–231}$), and mouse PrP 23–231 ($rMoPrP_{23–231}$)
316 in *Escherichia coli* strain BL21 (DE3) (Stratagene) was performed as previously
317 described [41]. The purified protein was stored at -80°C.

318 **SPRi screening**

319 SPR screening to discover drugs that bind to $rHuPrP_{90–231}$ was performed by Plexera
320 LCC (WA, USA). The screening subject was a library containing 1200 small molecules,
321 all of which were already approved drugs by the FDA and were selected for their high
322 chemical and pharmacological diversity, as well as for their known bioavailability and

safety in humans. The sample compounds, positive (10 mM rapamycin) and negative (DMSO) controls were printed on to the activated 3D sensor chip, and immobilized by a photo-crossing reaction. Excess unbound samples were eliminated by rinsing with dimethylformamide, ethanol, and H_2O, respectively. Sample analysis was prioritized using $rHuPrP_{90–231}$ (100, 200, 400, 800 nM), then FKBP12 (100 nM) as the positive control. The protein was injected once at a flow rate of 2 μL/s. The association duration was 300 sec and dissociation duration was 300 sec. Subsequent regeneration was performed using 900 μL of 10 mM glycine-HCl (pH 2.0). The assay was performed using Plexera PlexArray SPRi instrumentation, visualized using Instrument Control software, and analyzed using Plexera Data Explorer software.

Conventional SPR analysis

Conventional SPR analysis was performed using the Biacore T200 system (GE Healthcare Life Sciences). $rHuPrP_{23–231}$ and $rMoPrP_{23–231}$ were immobilized on a CM5 sensor chip (GE Healthcare Life Sciences) by amine coupling. Blank flow paths remained for background data. Two-fold serial dilutions of alprenolol hydrochloride, bisoprolol fumarate, and ampicillin (each at 625, 313, 156, 78, 39, 20, and 0 μM), and quinacrine (500, 250, 125, 62.5, 31.2, 15.6, 7.8, 3.9, and 0 μM) in running buffer (0.01 M HEPES pH 7.4, 0.15 M NaCl, 0.005% (v/v) Tween20) were injected for 120 sec at a

flow rate of 30 μL/min. After injection of each sample, the same buffer alone was injected for 60 sec at a flow rate of 30 μL/min for regeneration. Data were analyzed using Biacore T200 Evaluation software (GE Healthcare Life Sciences).

Nuclear magnetic resonance (NMR) measurement

For NMR measurements, recombinant mouse PrP 121–231 uniformly labeled with ^{15}N was prepared in 50 mM acetate-d_3 buffer (pH 4.8) containing 1 mM NaN_3 and 1 μM DSS dissolved in 99% H_2O/1% D_2O. NMR spectra were recorded at 25.0ºC on a Bruker Avance 600 spectrometer (Bruker BioSpin, Rheinstetten, Germany) at Gifu University. The spectrometer operated at a ^1H frequency of 600.13 MHz and a ^{15}N frequency of 60.81 MHz. A 5-mm ^1H inverse detection probe with triple-axis gradient coils was used for all measurements. ^1H-^{15}N HSQC spectra were acquired with 2048 complex points covering 9615 Hz for ^1H and 256 complex points covering 1521 Hz for ^{15}N. NMR data were processed using the TOPSPIN software package (Bruker BioSpin, Rheinstetten, Germany).

Docking simulation

We performed docking simulation of Alp and Oxp with mouse PrP^C using AutoDock 4.2 [36]. The three-dimensional structure of PrP^C obtained from the Protein Data Bank (ID: 1AG2 [42]) was used as a receptor. The atomic structures of Alp and Oxp were

359 downloaded from the PubChem website [43] (CID-66368 for alprenolol and CID-71172
360 for oxprenolol), and the atomic structures of their enantiomers were also generated. A
361 cubic space of 45 × 45 × 45 Å was used as a search region, covering the whole surface
362 of PrP^C. In our docking simulation, 50 individual calculations were run with genetic
363 algorithm (ga_run=50), in each of which 10^8 energy calculations were performed
364 (ga_num_evals=10^8). The lowest energy structure was selected as a potential binding
365 structure with PrP^C.

366 **Statistical analysis**

367 One-way analysis of variance (ANOVA) followed by the Tukey–Kramer test was
368 used for multiple comparisons. The log rank test was used to analyze the survival time
369 of mice. All statistical analyses were performed using Excel and GraphPad Prism
370 software.

371

References

1. Prusiner SB (1982) Novel proteinaceous infectious particles cause scrapie. Science 216 (4542):136-144

2. Prusiner SB (1998) Prions. Proc Natl Acad Sci U S A 95 (23):13363-13383

3. Rossi G, Salmona M, Forloni G, Bugiani O, Tagliavini F (2003) Therapeutic approaches to prion diseases. Clin Lab Med 23 (1):187-208

4. Weissmann C, Aguzzi A (2005) Approaches to therapy of prion diseases. Annu Rev Med 56:321-344. doi:10.1146/annurev.med.56.062404.172936

5. Aguzzi A, O'Connor T (2010) Protein aggregation diseases: pathogenicity and therapeutic perspectives. Nat Rev Drug Discov 9 (3):237-248. doi:10.1038/nrd3050

6. Vogtherr M, Grimme S, Elshorst B, Jacobs DM, Fiebig K, Griesinger C, Zahn R (2003) Antimalarial drug quinacrine binds to C-terminal helix of cellular prion protein. J Med Chem 46 (17):3563-3564. doi:10.1021/jm034093h

7. Doh-Ura K, Iwaki T, Caughey B (2000) Lysosomotropic agents and cysteine protease inhibitors inhibit scrapie-associated prion protein accumulation. J Virol 74 (10):4894-4897

8. Haïk S, Brandel JP, Salomon D, Sazdovitch V, Delasnerie-Lauprêtre N, Laplanche JL, Faucheux BA, Soubrié C, Boher E, Belorgey C, Hauw JJ, Alpérovitch A (2004) Compassionate use of quinacrine in Creutzfeldt-Jakob disease fails to show significant effects. Neurology 63 (12):2413-2415

9. Collinge J, Gorham M, Hudson F, Kennedy A, Keogh G, Pal S, Rossor M, Rudge P, Siddique D, Spyer M, Thomas D, Walker S, Webb T, Wroe S, Darbyshire J (2009) Safety and efficacy of quinacrine in human prion disease (PRION-1 study): a patient-preference trial. Lancet Neurol 8 (4):334-344. doi:S1474-4422(09)70049-3 [pii]
10.1016/S1474-4422(09)70049-3

10. Caughey B, Raymond GJ (1993) Sulfated polyanion inhibition of scrapie-associated PrP accumulation in cultured cells. J Virol 67 (2):643-650

11. Caughey B, Brown K, Raymond GJ, Katzenstein GE, Thresher W (1994) Binding of the protease-sensitive form of PrP (prion protein) to sulfated glycosaminoglycan and congo red [corrected]. J Virol 68 (4):2135-2141

12. Tsuboi Y, Doh-Ura K, Yamada T (2009) Continuous intraventricular infusion of pentosan polysulfate: clinical trial against prion diseases. Neuropathology 29 (5):632-636. doi:NEU1058 [pii]
10.1111/j.1440-1789.2009.01058.x

13. Doh-ura K, Ishikawa K, Murakami-Kubo I, Sasaki K, Mohri S, Race R, Iwaki T (2004) Treatment of transmissible spongiform encephalopathy by intraventricular drug infusion in

407 animal models. J Virol 78 (10):4999-5006
408 14. Bone I, Belton L, Walker AS, Darbyshire J (2008) Intraventricular pentosan
409 polysulphate in human prion diseases: an observational study in the UK. Eur J Neurol 15
410 (5):458-464. doi:10.1111/j.1468-1331.2008.02108.x
411 15. Haik S, Marcon G, Mallet A, Tettamanti M, Welaratne A, Giaccone G, Azimi S, Pietrini V,
412 Fabreguettes JR, Imperiale D, Cesaro P, Buffa C, Aucan C, Lucca U, Peckeu L, Suardi S,
413 Tranchant C, Zerr I, Houillier C, Redaelli V, Vespignani H, Campanella A, Sellal F,
414 Krasnianski A, Seilhean D, Heinemann U, Sedel F, Canovi M, Gobbi M, Di Fede G,
415 Laplanche JL, Pocchiari M, Salmona M, Forloni G, Brandel JP, Tagliavini F (2014)
416 Doxycycline in Creutzfeldt-Jakob disease: a phase 2, randomised, double-blind,
417 placebo-controlled trial. Lancet Neurol 13 (2):150-158. doi:10.1016/S1474-4422(13)70307-7
418 16. Tagliavini F, Forloni G, Colombo L, Rossi G, Girola L, Canciani B, Angeretti N,
419 Giampaolo L, Peressini E, Awan T, De Gioia L, Ragg E, Bugiani O, Salmona M (2000)
420 Tetracycline affects abnormal properties of synthetic PrP peptides and PrP(Sc) in vitro. J
421 Mol Biol 300 (5):1309-1322. doi:10.1006/jmbi.2000.3840
422 17. Forloni G, Iussich S, Awan T, Colombo L, Angeretti N, Girola L, Bertani I, Poli G,
423 Caramelli M, Grazia Bruzzone M, Farina L, Limido L, Rossi G, Giaccone G, Ironside JW,
424 Bugiani O, Salmona M, Tagliavini F (2002) Tetracyclines affect prion infectivity. Proc Natl
425 Acad Sci U S A 99 (16):10849-10854. doi:10.1073/pnas.162195499
426 162195499 [pii]
427 18. Peretz D, Williamson RA, Kaneko K, Vergara J, Leclerc E, Schmitt-Ulms G, Mehlhorn IR,
428 Legname G, Wormald MR, Rudd PM, Dwek RA, Burton DR, Prusiner SB (2001) Antibodies
429 inhibit prion propagation and clear cell cultures of prion infectivity. Nature 412
430 (6848):739-743. doi:10.1038/35089090
431 19. Heppner FL, Musahl C, Arrighi I, Klein MA, Rülicke T, Oesch B, Zinkernagel RM,
432 Kalinke U, Aguzzi A (2001) Prevention of scrapie pathogenesis by transgenic expression of
433 anti-prion protein antibodies. Science 294 (5540):178-182. doi:10.1126/science.1063093
434 20. White AR, Enever P, Tayebi M, Mushens R, Linehan J, Brandner S, Anstee D, Collinge J,
435 Hawke S (2003) Monoclonal antibodies inhibit prion replication and delay the development
436 of prion disease. Nature 422 (6927):80-83. doi:10.1038/nature01457
437 nature01457 [pii]
438 21. Solforosi L, Criado JR, McGavern DB, Wirz S, Sánchez-Alavez M, Sugama S, DeGiorgio
439 LA, Volpe BT, Wiseman E, Abalos G, Masliah E, Gilden D, Oldstone MB, Conti B,
440 Williamson RA (2004) Cross-linking cellular prion protein triggers neuronal apoptosis in
441 vivo. Science 303 (5663):1514-1516. doi:10.1126/science.1094273
442 22. Nakagaki T, Satoh K, Ishibashi D, Fuse T, Sano K, Kamatari YO, Kuwata K, Shigematsu

443 K, Iwamaru Y, Takenouchi T, Kitani H, Nishida N, Atarashi R (2013) FK506 reduces
444 abnormal prion protein through the activation of autolysosomal degradation and prolongs
445 survival in prion-infected mice. Autophagy 9 (9):1386-1394. doi:10.4161/auto.25381
446 23. Ishibashi D, Homma T, Nakagaki T, Fuse T, Sano K, Takatsuki H, Atarashi R, Nishida N
447 (2015) Strain-Dependent Effect of Macroautophagy on Abnormally Folded Prion Protein
448 Degradation in Infected Neuronal Cells. PLoS One 10 (9):e0137958.
449 doi:10.1371/journal.pone.0137958
450 24. Moreno JA, Halliday M, Molloy C, Radford H, Verity N, Axten JM, Ortori CA, Willis AE,
451 Fischer PM, Barrett DA, Mallucci GR (2013) Oral treatment targeting the unfolded protein
452 response prevents neurodegeneration and clinical disease in prion-infected mice. Sci Transl
453 Med 5 (206):206ra138. doi:10.1126/scitranslmed.3006767
454 25. Halliday M, Radford H, Sekine Y, Moreno J, Verity N, le Quesne J, Ortori CA, Barrett
455 DA, Fromont C, Fischer PM, Harding HP, Ron D, Mallucci GR (2015) Partial restoration of
456 protein synthesis rates by the small molecule ISRIB prevents neurodegeneration without
457 pancreatic toxicity. Cell Death Dis 6:e1672. doi:10.1038/cddis.2015.49
458 26. Kuwata K, Nishida N, Matsumoto T, Kamatari YO, Hosokawa-Muto J, Kodama K,
459 Nakamura HK, Kimura K, Kawasaki M, Takakura Y, Shirabe S, Takata J, Kataoka Y,
460 Katamine S (2007) Hot spots in prion protein for pathogenic conversion. Proc Natl Acad Sci
461 U S A 104 (29):11921-11926. doi:0702671104 [pii]
462 10.1073/pnas.0702671104
463 27. Hyeon JW, Choi J, Kim SY, Govindaraj RG, Jam Hwang K, Lee YS, An SS, Lee MK,
464 Joung JY, No KT, Lee J (2015) Discovery of Novel Anti-prion Compounds Using In Silico and
465 In Vitro Approaches. Sci Rep 5:14944. doi:10.1038/srep14944
466 28. Ishibashi D, Nakagaki T, Ishikawa T, Atarashi R, Watanabe K, Cruz FA, Hamada T,
467 Nishida N (2016) Structure-Based Drug Discovery for Prion Disease Using a Novel Binding
468 Simulation. EBioMedicine 9:238-249. doi:10.1016/j.ebiom.2016.06.010
469 29. Neumann T, Junker HD, Schmidt K, Sekul R (2007) SPR-based fragment screening:
470 advantages and applications. Curr Top Med Chem 7 (16):1630-1642
471 30. Nguyen HH, Park J, Kang S, Kim M (2015) Surface plasmon resonance: a versatile
472 technique for biosensor applications. Sensors (Basel) 15 (5):10481-10510.
473 doi:10.3390/s150510481
474 31. Pickhardt M, Neumann T, Schwizer D, Callaway K, Vendruscolo M, Schenk D, St
475 George-Hyslop P, Mandelkow EM, Dobson CM, McConlogue L, Mandelkow E, Tóth G (2015)
476 Identification of Small Molecule Inhibitors of Tau Aggregation by Targeting Monomeric Tau
477 As a Potential Therapeutic Approach for Tauopathies. Curr Alzheimer Res 12 (9):814-828
478 32. Pocchiari M, Schmittinger S, Masullo C (1987) Amphotericin B delays the incubation

479 period of scrapie in intracerebrally inoculated hamsters. J Gen Virol 68 (Pt 1):219-223.
480 doi:10.1099/0022-1317-68-1-219
481 33. Mangé A, Nishida N, Milhavet O, McMahon HE, Casanova D, Lehmann S (2000)
482 Amphotericin B inhibits the generation of the scrapie isoform of the prion protein in infected
483 cultures. J Virol 74 (7):3135-3140
484 34. Bühring KU, Sailer H, Faro HP, Leopold G, Pabst J, Garbe A (1986) Pharmacokinetics
485 and metabolism of bisoprolol-14C in three animal species and in humans. J Cardiovasc
486 Pharmacol 8 Suppl 11:S21-28
487 35. Hakkarainen JJ, Jalkanen AJ, Kääriäinen TM, Keski-Rahkonen P, Venäläinen T,
488 Hokkanen J, Mönkkönen J, Suhonen M, Forsberg MM (2010) Comparison of in vitro cell
489 models in predicting in vivo brain entry of drugs. Int J Pharm 402 (1-2):27-36.
490 doi:10.1016/j.ijpharm.2010.09.016
491 36. Morris GM, Huey R, Lindstrom W, Sanner MF, Belew RK, Goodsell DS, Olson AJ (2009)
492 AutoDock4 and AutoDockTools4: Automated docking with selective receptor flexibility. J
493 Comput Chem 30 (16):2785-2791. doi:10.1002/jcc.21256
494 37. Ashburn TT, Thor KB (2004) Drug repositioning: identifying and developing new uses for
495 existing drugs. Nat Rev Drug Discov 3 (8):673-683. doi:10.1038/nrd1468
496 38. Halliday M, Radford H, Zents KAM, Molloy C, Moreno JA, Verity NC, Smith E, Ortori
497 CA, Barrett DA, Bushell M, Mallucci GR (2017) Repurposed drugs targeting
498 eIF2α-P-mediated translational repression prevent neurodegeneration in mice. Brain.
499 doi:10.1093/brain/awx074
500 39. Yamamoto N, Kuwata K (2009) Regulating the conformation of prion protein through
501 ligand binding. J Phys Chem B 113 (39):12853-12856. doi:10.1021/jp905572w
502 40. Ishibashi D, Atarashi R, Fuse T, Nakagaki T, Yamaguchi N, Satoh K, Honda K, Nishida
503 N (2012) Protective Role of Interferon Regulatory Factor 3-Mediated Signaling against Prion
504 Infection. J Virol 86 (9):4947-4955. doi:JVI.06326-11 [pii]
505 10.1128/JVI.06326-11
506 41. Atarashi R, Moore RA, Sim VL, Hughson AG, Dorward DW, Onwubiko HA, Priola SA,
507 Caughey B (2007) Ultrasensitive detection of scrapie prion protein using seeded conversion
508 of recombinant prion protein. Nat Methods 4 (8):645-650. doi:10.1038/nmeth1066
509 42. Riek R, Hornemann S, Wider G, Billeter M, Glockshuber R, Wüthrich K (1996) NMR
510 structure of the mouse prion protein domain PrP(121-231). Nature 382 (6587):180-182.
511 doi:10.1038/382180a0
512 43. . https://pubchem.ncbi.nlm.nih.gov/.

513

Author contributions

Y.M., N.N., and R.A. designed the entire project. Y.M., T.I., Y.O.K, T.N., H.T., and D.I. performed the experiments and analyzed the data. N.N. and R.A. supervised and discussed the data. All authors reviewed the manuscript.

Conflict of Interest

The authors declare that there are no conflicts of interest.

525 **Figure legends**

526 **Fig. 1 Inhibitory effects of the candidate compounds on PrP^{Sc} accumulation in**

527 **N2a-FK cells**

528 (a) Structure of alprenolol hydrochloride, bisoprolol fumarate, colistin sulfate, esmolol

529 hydrochloride and oxprenolol hydrochloride. (b) Inhibitory effects of alprenolol

530 hydrochloride, bisoprolol fumarate and colistin sulfate on PrP^{Sc} accumulation in

531 N2a-FK cells. After the cells were incubated in medium mixed with each concentration

532 of sample compound or water (negative control) for 48 hours, the collected cell lysates

533 were digested with proteinase K. Western blotting was then performed for quantification

534 of the PrP^{Sc} level. (c) The intensity of each band was measured and expressed as a

535 percentage of the negative control. Data are presented as the mean ± SD of three

536 independent experiments. (d) Inhibitory effects of continued passage in the presence of

537 alprenolol hydrochloride, bisoprolol fumarate or colistin sulfate on PrP^{Sc} accumulation

538 in N2a-FK cells. The cells were cultured in medium mixed with 50 μM of alprenolol

539 hydrochloride, 100 μM of bisoprolol fumarate or 100 μM of colistin sulfate, or original

540 medium (negative control). The cells were passaged every 3 days and then the cell

541 lysates were collected. After digestion with proteinase K, western blotting was

542 performed to detect PrP^{Sc} accumulation. (e) PrP^{Sc} accumulation in N2a-FK cells after

543 treatment with esmolol hydrochloride and oxprenolol hydrochloride. After the cells had
544 been incubated in medium mixed with each concentration of sample compound or water
545 (negative control) for 48 hours, the collected cell lysates were digested with proteinase
546 K. Western blotting was then performed for quantification of the PrP^{Sc} level.
547
548 **Fig. 2 Alprenolol hydrochloride reduces PrP^{Sc} accumulation in a mouse brain at**
549 **115 d.p.i**
550 CD-1 mice were intracerebrally infected with strain Fukuoka-1. The following day, the
551 mice were given drinking water containing alprenolol hydrochloride at 250 mg/L or 50
552 mg/L. Mice in the control group were given normal drinking water without the
553 compound. At 115 d.p.i and the terminal stage, mice from each group were euthanized
554 for brain homogenates and histopathological analysis (control: n = 3; 250 mg/L: n = 5;
555 50 mg/L: n = 3). (a) Western blotting of the brain homogenates at 115 d.p.i. was
556 performed to quantify the PrP^{Sc} level. The intensity of each band was measured and
557 expressed as a percentage of the control. The data are presented as the mean ± SD.
558 Statistical analysis was determined using one-way ANOVA followed by the Tukey–
559 Kramer test. ***$p < 0.001$ compared with the control. (b) Immunohistochemical
560 staining of PrP^{Sc} of the brain slices at 115 d.p.i was performed. Scale bar: 100 μm.

561

562 **Fig. 3 Effects of alprenolol hydrochloride on the spongiform changes in mouse**

563 **brains at 115 d.p.i.**

564 Hematoxylin and eosin staining of PrP^{Sc} in the brain sections at 115 d.p.i was performed.

565 The areas occupied by vacuoles were quantified using ImageJ software (cortex: Cx,

566 hippocampus: Hip, thalamus: Tha, striatum: St). The data are presented as the mean ±

567 SD. Statistical analysis was determined using one-way ANOVA followed by the Tukey–

568 Kramer test. *$p < 0.05$ compared with the control. Scale bar: 100 μm.

569

570 **Fig. 4 Docking simulation of the interaction of alprenolol and oxprenolol with**

571 **mouse PrP^{C}**

572 Binding structures obtained by the docking simulation for alprenolol and its enantiomer

573 (a), and oxprenolol and its enantiomers (b). PrP^{C}, including three helixes (HA, HB and

574 HC), is shown by a ribbon representation in light blue, and the compounds are shown by

575 stick models. The calculated binding energies are also given.

576

577 **Supplementary Fig. 1 Effects of the candidate compounds on PrP^{Sc} accumulation**

578 **in N2a-FK cells**

579 PrP^{Sc} accumulation in N2a-FK cells after treatment with the SPRi hit compounds. These
580 27 compounds were not effective in PrP^{Sc} accumulation. After the cells had been
581 incubated in medium mixed with each concentration of sample compound for 48 hours,
582 the collected cell lysates were digested with proteinase K. Western blotting was then
583 performed for quantification of the PrP^{Sc} level.
584
585 **Supplementary Fig. 2 Histological analysis of the mouse brain at the terminal stage**
586 (a) Survival curves in the Fukuoka-1-infected mice administered Alp. The control mice
587 (n = 7) and Alp-treated mice (250 mg/L: n = 9; 50 mg/L: n = 10) were compared. At the
588 terminal stage, mice from each group were euthanized for brain homogenates and
589 histopathological analysis (Control: n = 4; 250 mg/L: n = 4; 50 mg/L: n = 4). (b)
590 Western blotting of the brain homogenates and (c) hematoxylin and eosin staining of the
591 brain slices were performed. Scale bars: 100 μm.
592
593 **Supplementary Fig. 3 Binding activity of the candidate compounds to $rMoPrP_{23–231}$**
594 Binding affinity of $rMoPrP_{23–231}$ with each candidate compound was examined using the
595 Biacore T200. (a) Sensorgrams and (b) affinity curves of alprenolol hydrochloride,
596 bisoprolol fumarate, ampicillin and quinacrine for $rMoPrP_{23–231}$. The concentrations of

alprenolol hydrochloride, bisoprolol fumarate and ampicillin were 625, 313, 156, 78, 39, 20 and 0 μM and those of quinacrine were 500, 250, 125, 62.5, 31.2, 15.6, 7.8, 3.9 and 0 μM from top to bottom in the sensorgrams.

Supplementary Fig. 4 Binding activity of the candidate compounds to rHuPrP$_{23–231}$

Binding affinity between rHuPrP$_{23–231}$ and each candidate compound was examined using the Biacore T200. (a) Sensorgrams and (b) affinity curves of alprenolol hydrochloride, bisoprolol fumarate, ampicillin, and quinacrine for rHuPrP$_{23–231}$. The concentrations of alprenolol hydrochloride, bisoprolol fumarate, and ampicillin were 625, 313, 156, 78, 39, 20, and 0 μM and those of quinacrine were 500, 250, 125, 62.5, 31.2, 15.6, 7.8, 3.9, and 0 μM from top to bottom in the sensorgrams.

Supplementary Fig. 5 NMR analysis to evaluate alprenolol HCl binding

^{1}H-^{15}N HSQC spectra of the ^{15}N-labeled recombinant mouse PrP 121–231 (200 μM), with (red) or without (blue) Alp (4 mM) at pH 4.8 and 25.0ºC.

Tables

Table 1: Hit compounds by SPRi screening

	Drugs	AvgK$_D$ (M)	Avg k_a (1/Ms)	Avg k_d (1/s)	Therapeutic class	Therapeutic effect
1	**Esmolol hydrochloride**	1.77×10^{-10}	1.58×10^{5}	2.81×10^{-5}	Cardiovascular	Antiarrhythmic
2	**Alexidine dihydrochloride**	2.26×10^{-10}	1.76×10^{3}	3.97×10^{-7}	Infectiology	Antibacterial
3	**Dequalinium dichloride**	4.81×10^{-10}	285	1.37×10^{-7}	Infectiology	Antibacterial
4	**Demecarium bromide**	1.69×10^{-9}	2.14×10^{3}	3.60×10^{-6}	Ophthalmology	Antiglaucoma
5	**Bisoprolol fumarate**	2.78×10^{-9}	307	8.54×10^{-7}	Cardiovascular	Antianginal
6	**Benzbromarone**	3.45×10^{-9}	1.10×10^{5}	3.78×10^{-4}	Cardiovascular	Antianginal
7	**Atractyloside potassium salt**	3.58×10^{-9}	2.68×10^{5}	9.59×10^{-4}	Oncology	Antineoplastic
8	**Fosinopril**	5.46×10^{-9}	7.04×10^{4}	3.84×10^{-4}	Cardiovascular	Antihypertensive
9	**Merbromin**	6.50×10^{-9}	72.7	4.72×10^{-7}	Infectiology	Antibacterial
10	**Furosemide**	7.25×10^{-9}	9.12×10^{4}	6.61×10^{-4}	Metabolism	Antihypertensive
11	**Etifenin**	1.00×10^{-8}	1.00×10^{3}	1.00×10^{-5}	Diagnostic	Chemosensitizer
12	**Acemetacin**	1.04×10^{-8}	5.19×10^{4}	5.42×10^{-4}	Metabolism	Anti-inflammatory
13	**Candesartan**	1.05×10^{-8}	2.06×10^{3}	2.17×10^{-5}	Cardiovascular	Antihypertensive
14	**Amphotericin B**	1.11×10^{-8}	1.59×10^{5}	1.75×10^{-3}	Infectiology	Antibacterial
15	**Alprenolol hydrochloride**	1.14×10^{-8}	4.86×10^{4}	5.53×10^{-4}	Cardiovascular	Antianginal
16	**Ketoprofen**	1.23×10^{-8}	1.68×10^{5}	2.07×10^{-3}	Central Nervous System	Analgesic
17	**Bumetanide**	1.43×10^{-8}	1.61×10^{5}	2.31×10^{-3}	Metabolism	Diuretic
18	**Triprolidine hydrochloride**	1.67×10^{-8}	6.08×10^{4}	1.02×10^{-3}	Allergology	Antihistaminic
19	**Methacycline hydrochloride**	1.92×10^{-8}	244	4.67×10^{-6}	Metabolism	Antibacterial
20	**Cefoperazone dihydrate**	2.36×10^{-8}	1.39×10^{5}	3.28×10^{-3}	Infectiology	Antibacterial
21	**Colistin sulfate**	2.37×10^{-8}	6.42×10^{4}	1.52×10^{-3}	Infectiology	Antibacterial
22	**Cefixime**	2.39×10^{-8}	7.60×10^{4}	1.82×10^{-3}	Infectiology	Antibacterial
23	**Tranilast**	2.43×10^{-8}	4.44×10^{4}	1.08×10^{-3}	Allergology	Antiallergic
24	**Norfloxacin**	2.45×10^{-8}	3.90×10^{4}	9.54×10^{-4}	Infectiology	Antibacterial
25	**Antimycin A**	5.57×10^{-8}	6.18×10^{4}	3.45×10^{-3}	Infectiology	Antibacterial
26	**Cefotetan**	7.85×10^{-8}	2.44×10^{4}	1.91×10^{-3}	Infectiology	Antibacterial
27	**Indomethacin**	1.04×10^{-7}	6.81×10^{4}	7.09×10^{-3}	Central Nervous System	Analgesic
28	**Doxepin hydrochloride**	1.49×10^{-7}	3.30×10^{4}	4.91×10^{-3}	Allergology	Anticonvulsant
29	**Oxprenolol hydrochloride**	3.08×10^{-7}	32.7	1.01×10^{-5}	Cardiovascular	Antianginal
30	**Ethacrynic acid**	9.54×10^{-7}	582	5.55×10^{-4}	Metabolism	Diuretic
31	**Rebamipide**	1.86×10^{-6}	338	6.29×10^{-4}	Metabolism	Antiulcer

In total, 31 compounds with an K_D value less than 1×10^{-6} M were listed as hit

compounds.

Table 2: Survival periods of prion-infected mice administered alprenolol hydrochloride

Mouse	Strain	Alprenolol HCl (mg/L)	Number	Mean ± SD (days)
CD-1	Fukuoka-1	0	7	168.4 ± 7.2
		250	9	164 ± 12.4
		50	10	162 ± 10.3

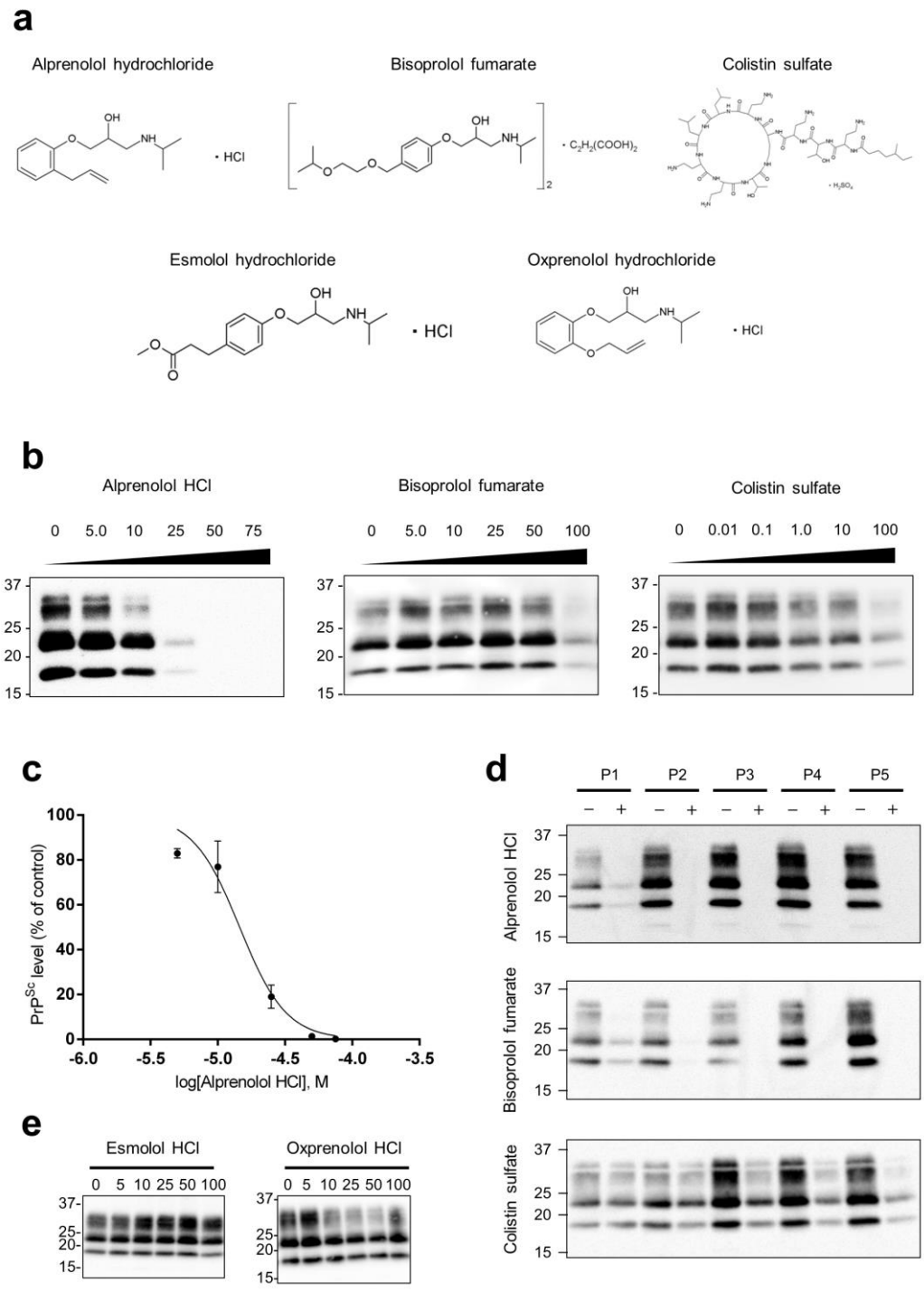
a
Alprenolol hydrochloride
Bisoprolol fumarate
Colistin sulfate
Esmolol hydrochloride
Oxprenolol hydrochloride
b
Alprenolol HCl
Bisoprolol fumarate
Colistin sulfate
c
PrP^Sc level (% of control)
log[Alprenolol HCl], M
d
P1
P2
P3
P4
P5
Alprenolol HCl
Bisoprolol fumarate
Colistin sulfate
e
Esmolol HCl
Oxprenolol HCl

Fig. 1

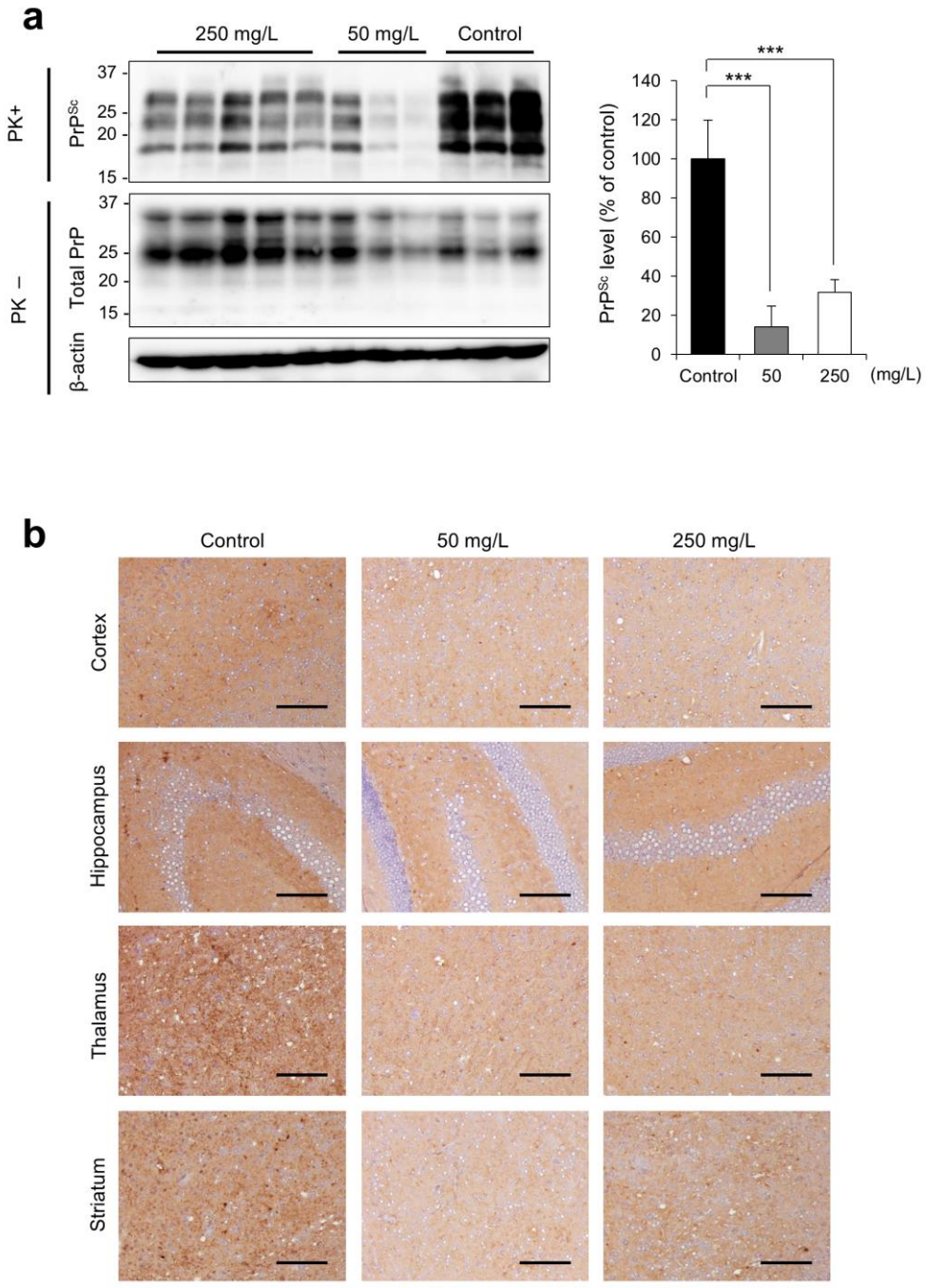
a
250 mg/L
50 mg/L
Control
PK+
PK –
PrPSc
Total PrP
β-actin
37
25
20
15
***
***
140
120
100
80
60
40
20
0
PrPSc level (% of control)
Control
50
250
(mg/L)
b
Control
50 mg/L
250 mg/L
Cortex
Hippocampus
Thalamus
Striatum

Fig. 2

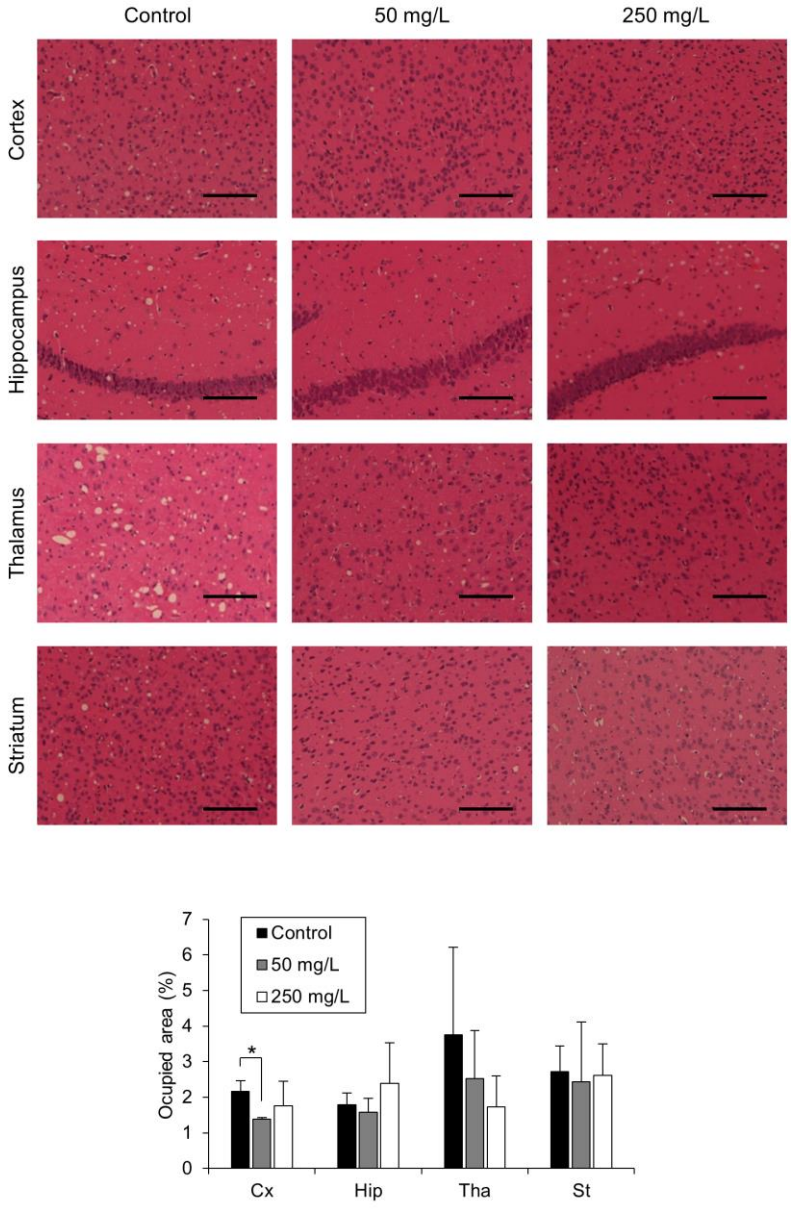
Control
50 mg/L
250 mg/L
Cortex
Hippocampus
Thalamus
Striatum
Control
50 mg/L
250 mg/L
Ocupied area (%)
0
1
2
3
4
5
6
7
*
Cx
Hip
Tha
St

Fig. 3

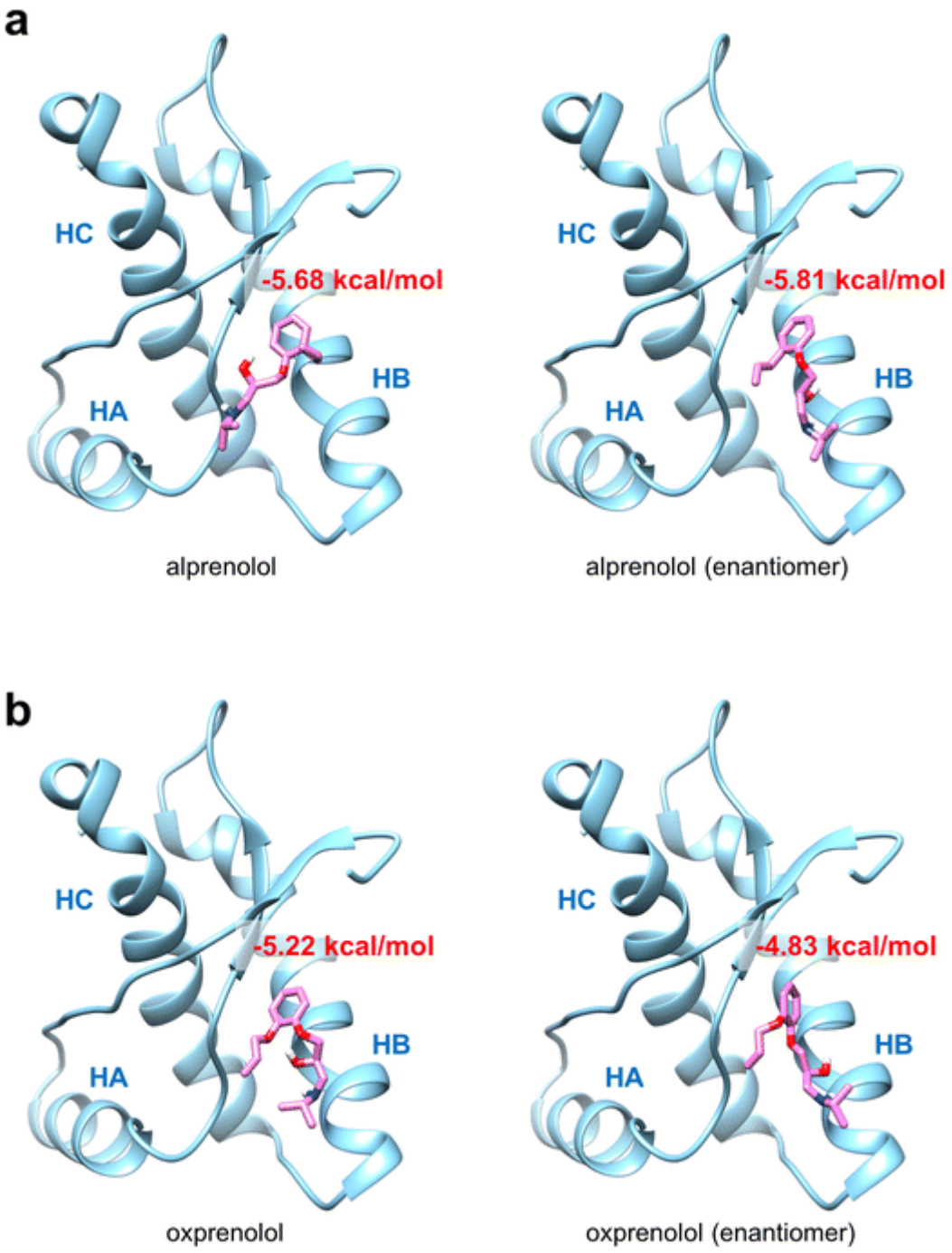
a
HC
-5.68 kcal/mol
HB
HA
alprenolol
HC
-5.81 kcal/mol
HB
HA
alprenolol (enantiomer)
b
HC
-5.22 kcal/mol
HB
HA
oxprenolol
HC
-4.83 kcal/mol
HB
HA
oxprenolol (enantiomer)

Fig. 4

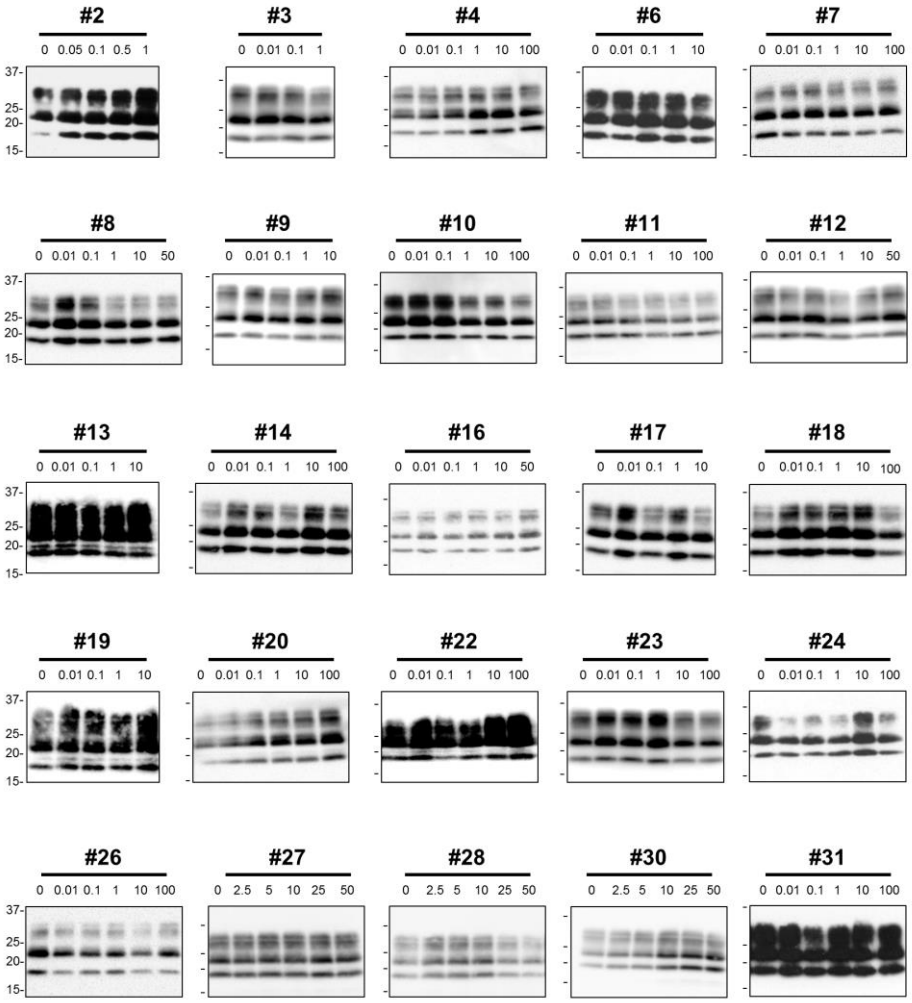
#2
0 0.05 0.1 0.5 1
#3
0 0.01 0.1 1
#4
0 0.01 0.1 1 10 100
#6
0 0.01 0.1 1 10
#7
0 0.01 0.1 1 10 100
#8
0 0.01 0.1 1 10 50
#9
0 0.01 0.1 1 10
#10
0 0.01 0.1 1 10 100
#11
0 0.01 0.1 1 10 100
#12
0 0.01 0.1 1 10 50
#13
0 0.01 0.1 1 10
#14
0 0.01 0.1 1 10 100
#16
0 0.01 0.1 1 10 50
#17
0 0.01 0.1 1 10
#18
0 0.01 0.1 1 10 100
#19
0 0.01 0.1 1 10
#20
0 0.01 0.1 1 10 100
#22
0 0.01 0.1 1 10 100
#23
0 0.01 0.1 1 10 100
#24
0 0.01 0.1 1 10 100
#26
0 0.01 0.1 1 10 100
#27
0 2.5 5 10 25 50
#28
0 2.5 5 10 25 50
#30
0 2.5 5 10 25 50
#31
0 0.01 0.1 1 10 100
37-
25-
20-
15-

Fig. S1

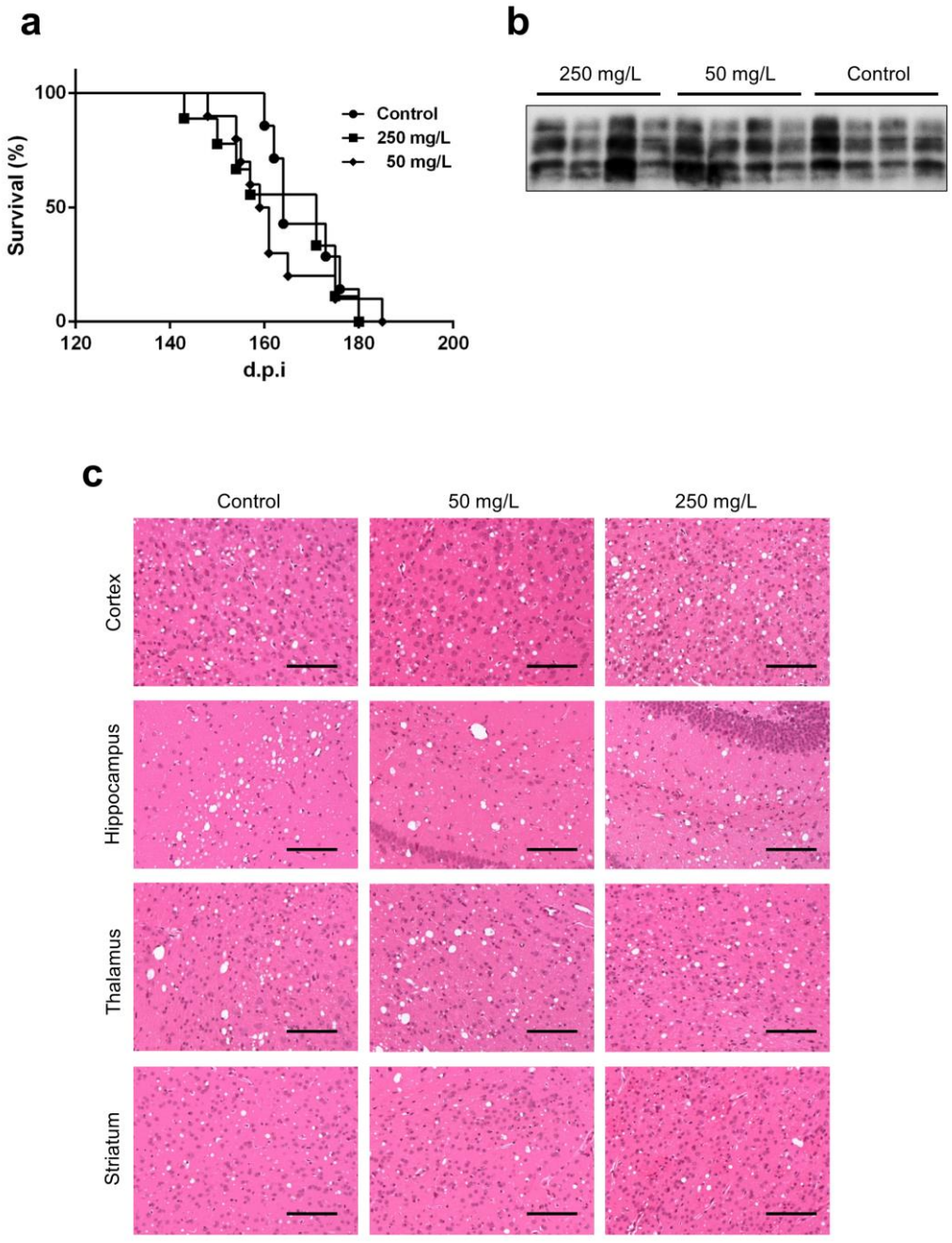
a
100
50
0
Survival (%)
120
140
160
180
200
d.p.i
Control
250 mg/L
50 mg/L
b
250 mg/L
50 mg/L
Control
c
Control
50 mg/L
250 mg/L
Cortex
Hippocampus
Thalamus
Striatum

Fig. S2

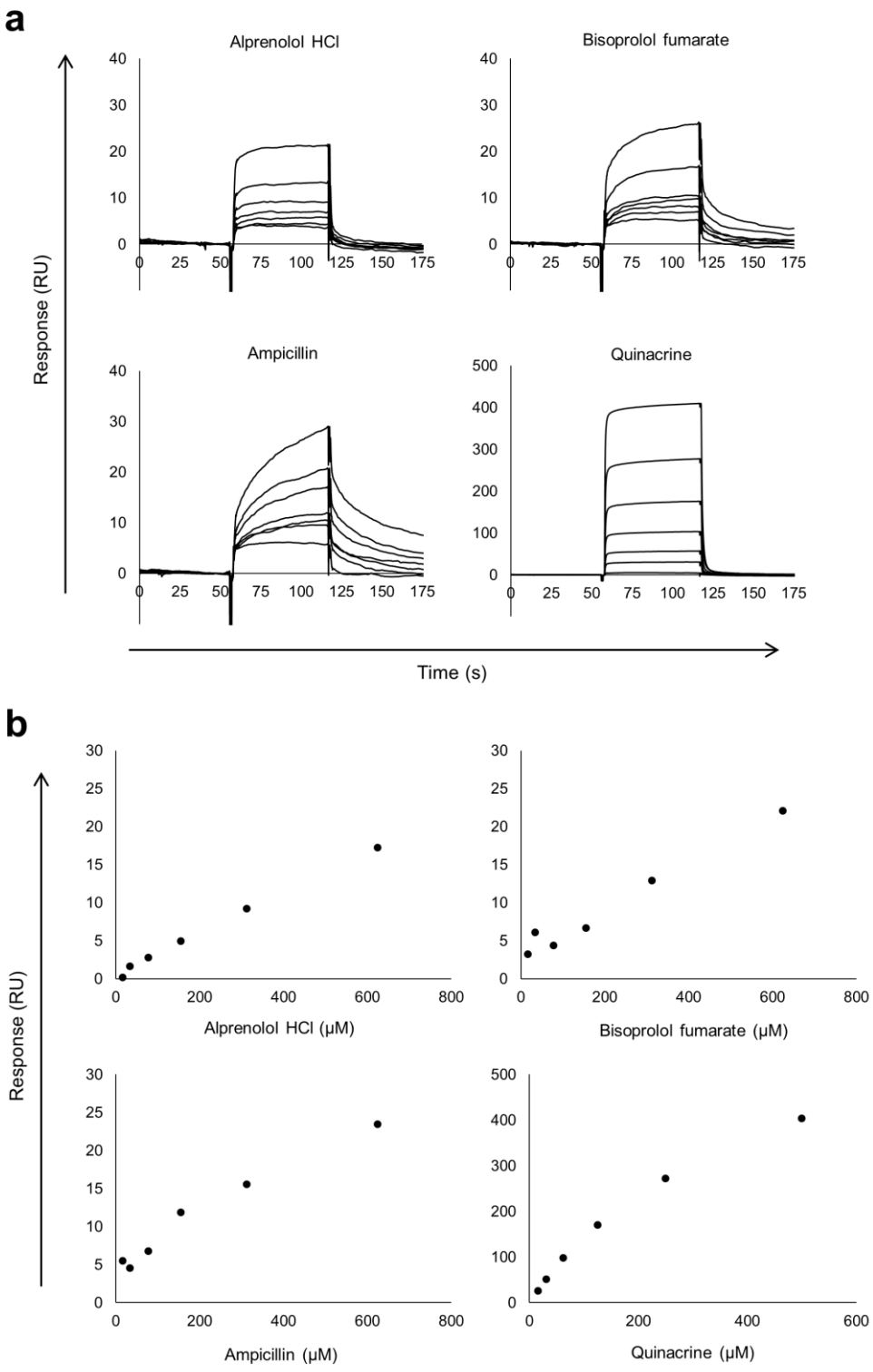
a
Alprenolol HCl
Bisoprolol fumarate
Ampicillin
Quinacrine
Response (RU)
Time (s)
b
Response (RU)
Alprenolol HCl (μM)
Bisoprolol fumarate (μM)
Ampicillin (μM)
Quinacrine (μM)

Fig. S3

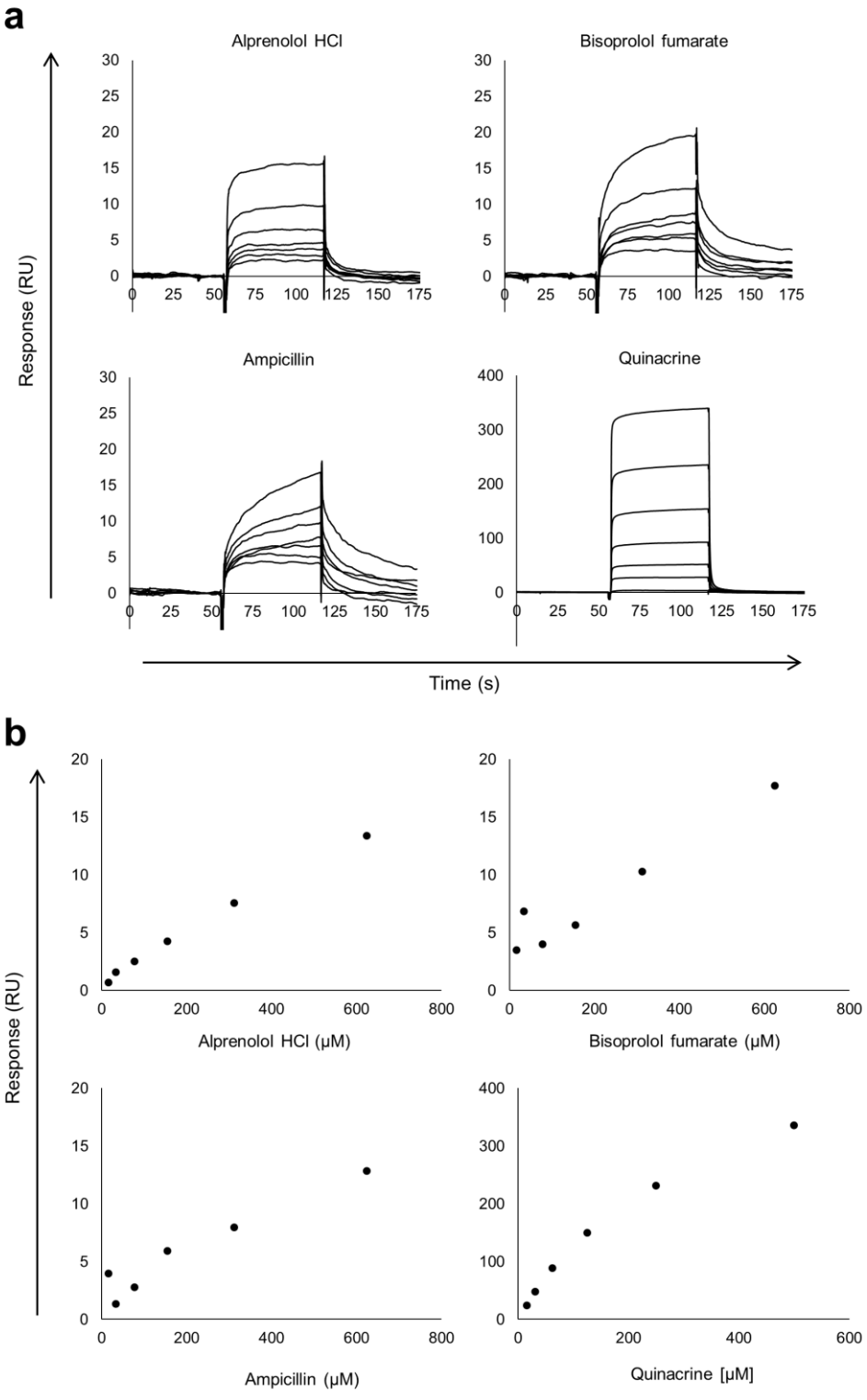
a
Alprenolol HCl
Bisoprolol fumarate
Ampicillin
Quinacrine
Response (RU)
Time (s)
b
Response (RU)
Alprenolol HCl (μM)
Bisoprolol fumarate (μM)
Ampicillin (μM)
Quinacrine [μM]

Fig. S4

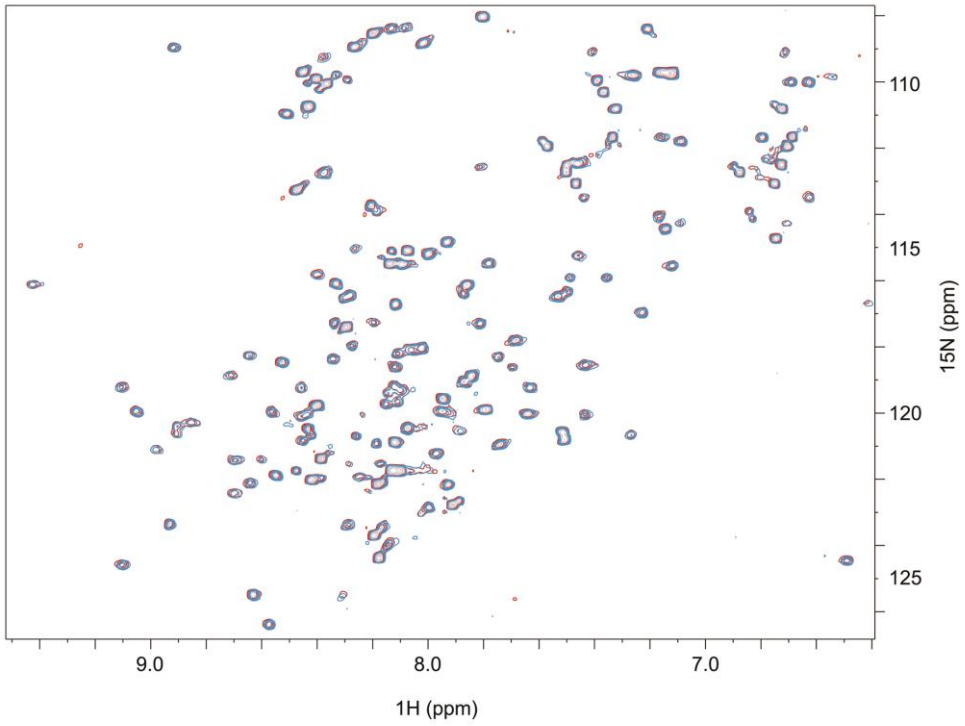

Fig. S5